Myocardial disarray drives metabolic inefficiency in human cardiomyocytes

Short title: Myocardial disarray and cardiac energetics

Charlène Jouve[1], Andrea Ruiz-Velasco[1], Erminia Donnarumma[2], Rémi Le Borgne[3], Iman Momken[4], Céline Pereira[1], Magali Seguret[1], Eva Vermersch[1], Elodie Vimont[2], Ivan Nemazanyy[5], Luc Bertrand[7], Timothy Wai[2], Jean-Marc Verbavatz[3], Mathias Mericksay[4], Jean-Sébastien Hulot[1,7*]

[1] Université de Paris Cité, Paris Cardiovascular Research Center, INSERM U970, F-75015 Paris, France;
[2] Institut Pasteur, Mitochondrial Biology Unit, CNRS UMR 3691, Université Paris Cité, Paris, France ;
[3] Université Paris Cité, CNRS, Institut Jacques Monod, F-75013 Paris, France;
[4] Department of Signaling and Cardiovascular Pathophysiology, UMR-S 1180, Inserm, Université Paris-Saclay, France;
[5] Platform for Metabolic Analyses, Structure Fédérative de Recherche Necker, INSERM US24/CNRS UAR 3633, Paris, France;
[6] Pôle de Recherche Cardiovasculaire (CARD), Institut de Recherche Expérimentale et Clinique (IREC), Université catholique de Louvain (UCLouvain), Brussels, Belgium
[7] CIC1418 and DMU CARTE, AP-HP, Hôpital Européen Georges Pompidou, F-75015, Paris, France

Supplementary material

- **Supplementary Tables : 3**
- **Supplementary Figures : 8**

Supplementary Table 1. 16 entities identified in the carnitine metabolism pathway from the REACTOME Pathway Analysis. Up/down expressions correspond to changes of plus or minus 30% respectively.

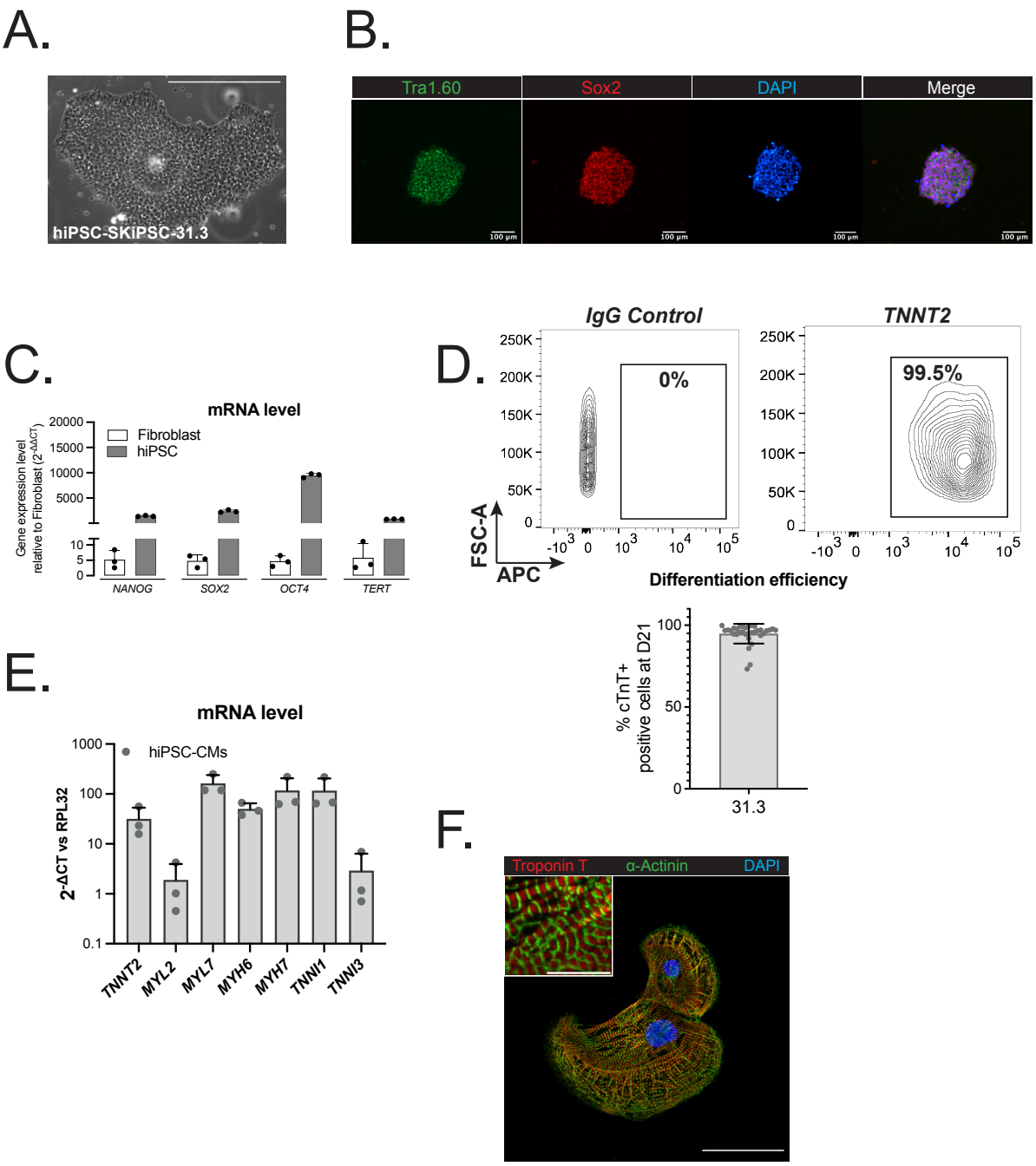
Gene	UniPro Id	logFC	Interpretation
ACACA	Q13085	-0,17461268	down
ACACB	O00763	0,09898097	
CPT1A	P50416	0,243642567	up
CPT1B	Q92523	0,222166436	up
CPT2	P23786	0,085895949	
MID1IP1	Q9NPA3	-0,213965579	down
PPARD	Q03181	-0,152778742	down
PRKAA2	P54646	0,052515816	
PRKAB2	O43741	0,002802349	
PRKAG2	Q9UGJ0	0,091991203	
RGMB	O00863	-0,128303368	
RXRA	P19793	0,055295189	
SLC22A4	O76082	-0,178795184	down
SLC22A5	O76082	-0,162658222	down
SLC25A20	O43772	0,102333938	
THRSP	Q92748	1,252323355	

Supplementary Table 2. Antibodies used for Immunofluorescence (IF), duolink PLA, Flow cytometry (FC) and Western blot (WB).

Antibodies	Manufacturer	Assay	Cat. No.	Dilution
cTnT, APC, REAfinity	Miltenyi Biotech	FC	130-120-403	1:100
REA control human IgG1, APC, REAfinity	Miltenyi Biotech	FC	130-120-709	1:100
Cardiac Troponin T	Abcam	IF	Ab45932	1:500
Alpha-actinin	Sigma-Aldrich	IF	A7811	1:1000
Connexin 43	Thermo Fisher Scientific	IF	71-0700	1:200
TRA-1-60	Millipore	IF	MAB4360	1:100
SOX2	Millipore	IF	AB5603	1:200
VDAC1	Abcam	PLA/WB	Ab14734	1:200/1:1000
IP_3R1	Millipore	PLA	07-1213	1:100
GRP75	Cell Signaling	PLA/WB	3593	1:100/1:1000
GRP75	Santa Cruz	PLA	Sc-133137	1:100
IP_3R1	Cell Signaling	WB	8568	1:1000
VDAC	Thermo Fisher Scientifc	WB	PA1-954A	1:1000
OPA1	BD Biosciences	WB	612607	1:1000
TOMM40	Proteintech Group	WB	18409-1-AP	1:1000
Total OXPHOS cocktail	Abcam	WB	Ab110411	1:1000
SDHA	Invitrogen	WB	459200	1:500
Histone H3	Abcam	WB	Ab1791	1:1000
Vinculin	Sigma Aldrich	WB	V9131	1:5000
AMPKα	Cell Signaling	WB	5831	1:1000
ACC	Cell Signaling	WB	3676	1:1000
p-AMPK(Thr172)	Cell Signaling	WB	2535	1:1000
p-ACC(Ser79)	Cell Signaling	WB	3661	1:1000
MCU	Cell Signaling	WB	14994	1:1000
MICU1	Thermo Fisher Scientific	WB	PA5-57966	1:1000
Donkey anti-Rabbit HRP Conjugated	Jackson ImmunoResearch	WB	711-035-152	1:10,000
Donkey anti-Mouse HRP Conjugated	Jackson ImmunoResearch	WB	715-035-150	1:10,000
Goat anti-Rabbit IgG Heavy and Light Chain HRP	Euromedex	WB	BE-A120-101P	1:10,000
Goat anti-Mouse IgG Heavy and Light Chain HRP	Euromedex	WB	BE-A90-116P	1:10,000
Goat anti-Rabbit IgG (H+L), Alexa Fluor® 546	Thermo Fisher Scientific	IF	A11010	1:1000
Goat anti-Mouse IgG (H+L), Alexa Fluor® 488	Thermo Fisher Scientific	IF	A10680	1:1000

Supplementary Table 3. List of primers.

Target	Forward primer	Reverse primer	Product
RPL32	AGTTCCTGGTCCACAACGTC	GTGACTCTGATGGCCAGTTG	142
NANOG	CTCCAACATCCTGAACCTCAGC	CGTCACACCATTGCTATTCTTCG	115
SOX2	GCCCTGCAGTACAACTCCAT	GACTTGACCACCGAACCCAT	128
OCT4 (POU5F1)	AATTTGTTCCTGCAGTGCCC	CTCTCGTTGTGCATAGTCGC	150
hTERT	CAAGCTGTTTGCGGGGATTC	AGTTCACCACTGTCTTCCGC	167
TNNT2	CAGGATCAACGATAACCAGAAAGTC	GTGAAGGAGGCCAGGCTCTA	87
MYL2	GCAGGCGGAGAGGTTTTC	AGTTGCCAGTCACGTCAGG	74
MYL7	CCGTCTTCCTCACGCTCTT	TGAACTCATCCTTGTTCACCAC	120
MYH6	TCTCCGACAACGCCTATCAGTAC	GTCACCTATGGCTGCAATGCT	140
MYH7	GGCAAGACAGTGACCGTGAAG	CGTAGCGATCCTTGAGGTTGTA	133
TNNI1	TCCGTGGGAAGTTCAAGCG	GACTTGGCGGCATCAAACATC	238
TNNI3	CCAACTACCGCGCTTATGC	CTCGCTCCAGCTCTTGCTTT	120
MT-TL1	CGAAAGGACAAGAGAAATAGAG	GAACAAGGTTTTAAGTCTTACGCA	134
b-Actin	GTGACGTTGACATCCGTAAAGA	CCTCACCAAGCTAAGGATGC	250



Supplementary Figure 1: hiPSC and hiPSC-CMs characterization.

A. Representative phase-contrast image of the hiPSC cells. Scale bar 400 µm.

B. Representative immunostaining in the hiPSC cells for Tra1.60 (green), and Sox2 (red). DAPI (blue) was used to stain nuclei. Scale bar 100 µm.

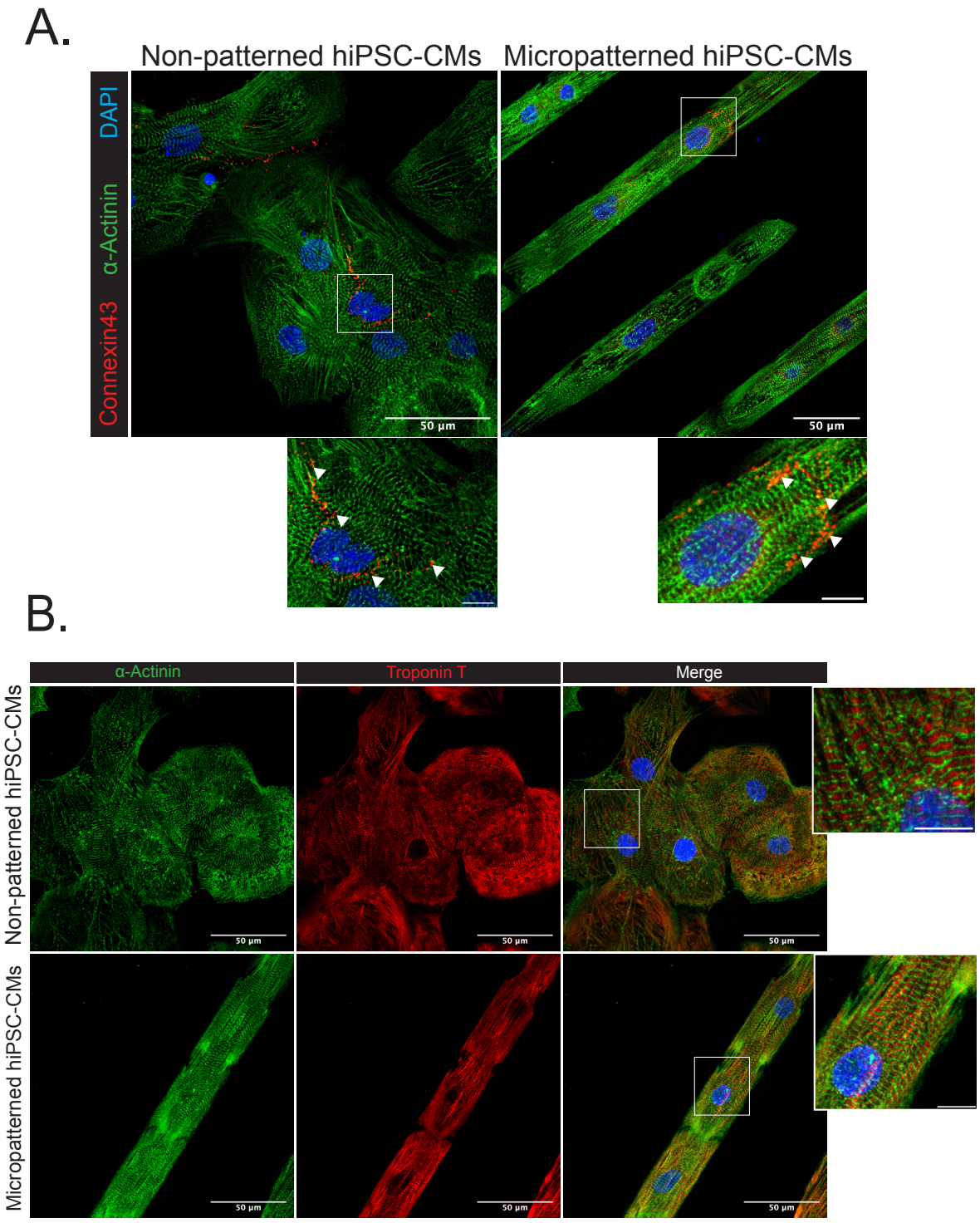
C. Relative mRNA levels of pluripotency markers in hiPSC cells normalized to normal human dermal fibroblasts.

D. Upper: Contour plot of hiPSC-CMs with TNNT2 staining analysed by FACS to calculate cardiac differentiation efficiency. 30,000 events recorded per group. Lower: Cardiac differentiation

efficiency was calculated by the percentage of $TNNT2^{+}$ cells after 21 days of differentiation; n = 10 batches per group.

E. Relative mRNA levels of cardiac markers hiPSC-CMs normalized to *RPL32*. N = 3 differentiations.

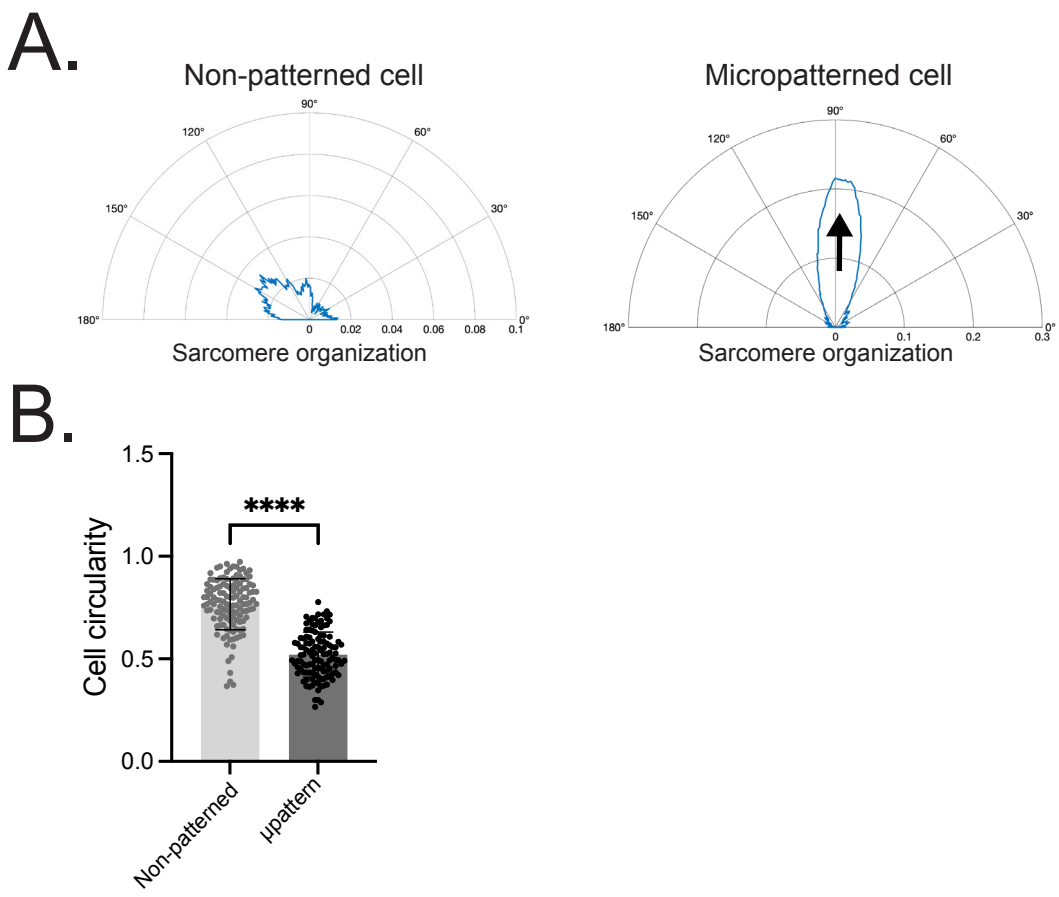
F. Representative immunofluorescence images of hiPSC-CMs, for alpha-sarcomeric actinin (green), cardiac Troponin T2 (red) at day 30 after differentiation. DAPI (blue) was used to stain nuclei. The insert represents a zoomed view of sarcomeres. Global scale bar 50 µm, insert scale bar 10 µm.



Supplementary Figure 2: Comparison of sarcomeric structures in non-patterned and micropatterned hiPSC-CMs.

A. Non-patterned and micropatterned hiPSC-CMs stained with alpha-sarcomeric actinin (green) and connexin43 (red) 7 days after seeding. DAPI (blue) was used to stain nuclei. The insert represents a zoomed view of cell connection, scale bar 10 µm.

B. Non-patterned and micropatterned hiPSC-CMs stained with alpha-sarcomeric actinin (green) and cardiac Troponin T2 (red) 7 days after seeding. DAPI (blue) was used to stain nuclei. The insert represents a zoomed view of sarcomeres, scale bar 10 μm.

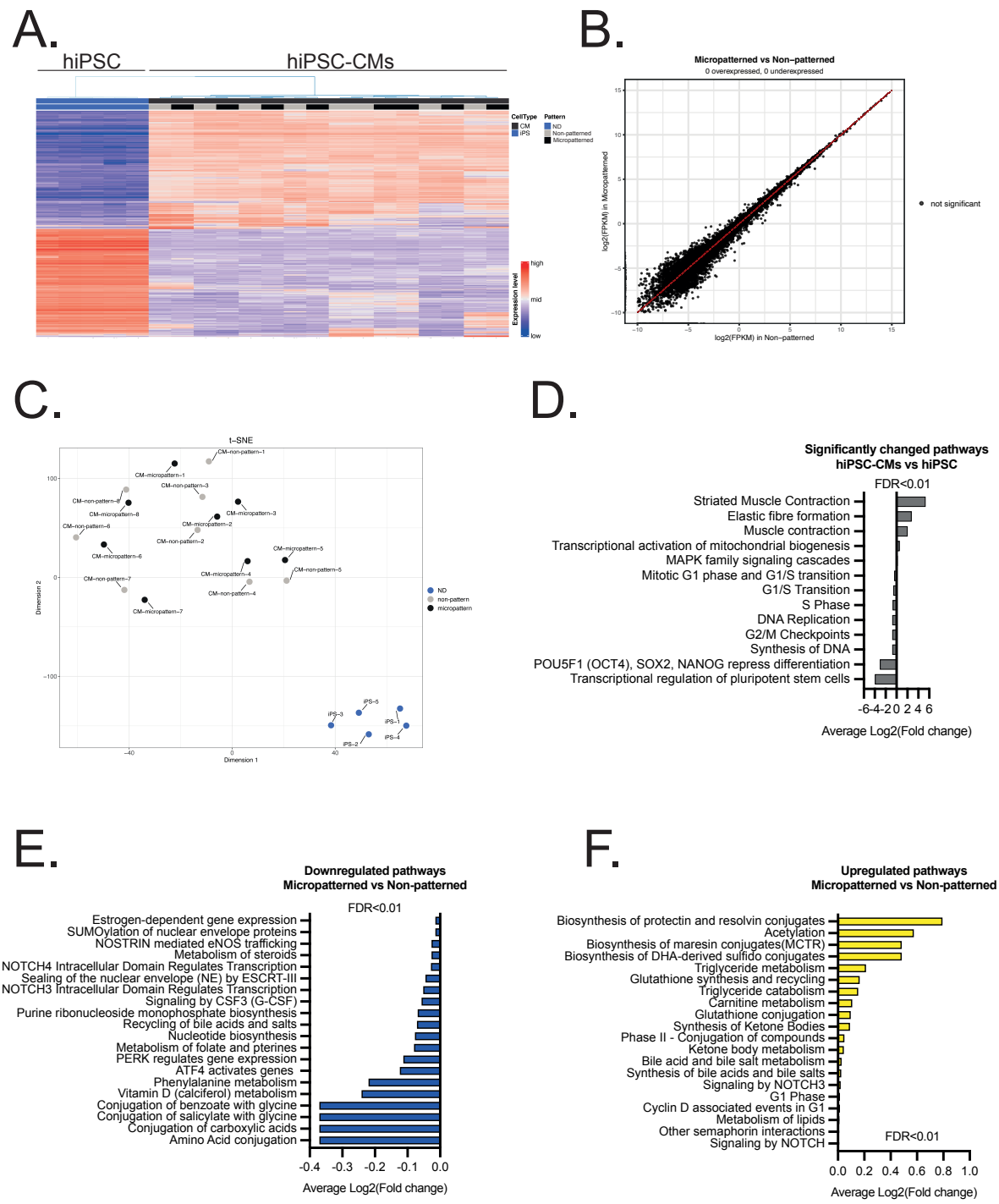


Supplementary Figure 3: Automated measures of sarcomere organization

A. Haralick correlation metric computed at multiple offset distances and angles to determine sarcomere organization and sarcomere length. Sarcomere organization assessed as a function of angle to assess the primary direction of sarcomere alignment. Arrow points in the direction of sarcomere alignment.

B. Scatter plot shows cell circularity, measured with automated morphology measurements. n = 138 non-patterned cells, n = 120 micropatterned cells; N = 3-4 differentiations.

Results, mean ± standard deviation. Statistical analyses: Unpaired t test was used for B. ****p<0.0001 for the comparisons indicated.



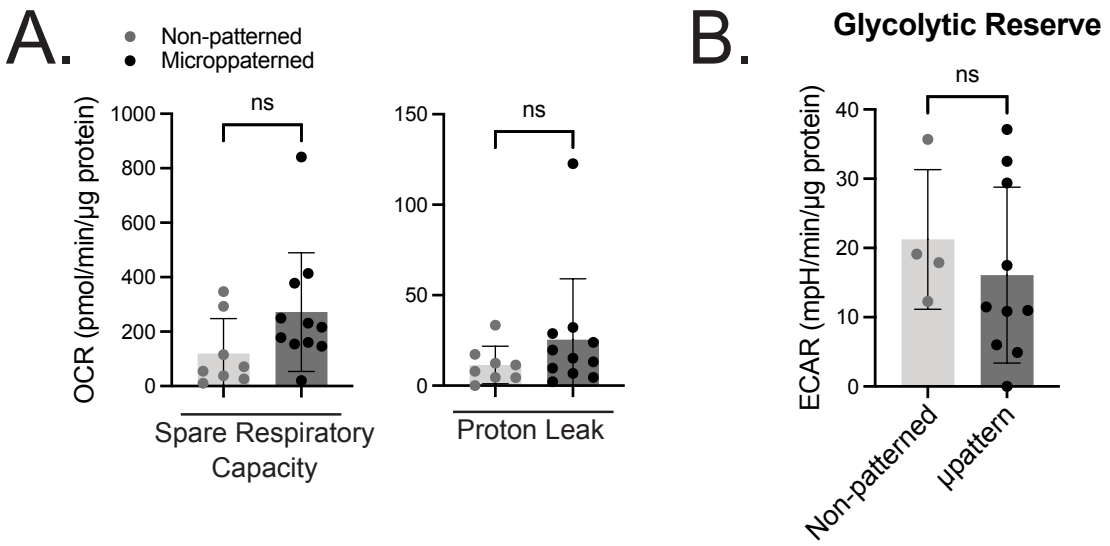
Supplementary Figure 4: Significantly up- and down-regulated pathways in micropatterned hiPSC-CMs compared to non-patterned hiPSC-CMs.

A. Heatmap of gene expression showing hierarchical clustering of hiPSC and hiPSC-CMs cells (micropatterned and non-patterned) detected by RNA-seq. N=5-8 differentiations.

B. Scatterplot depicting the Log2(FPKM) gene expression of micropatterned vs. non-patterned hiPSC-CMs. Black dots indicate no significant differential expression.

C. tSNE plot of iPSC (blue), iPSC-CMs non-patterned (grey), and micropatterned (black) clusters.

D. Representative significantly changed pathways (FDR>0.01) between hiPSC-CM and hiPSC as found with ReactomeGSA pathway analysis. Data presented as the average Log2(Fold change).
E. All significantly downregulated pathways (FDR<0.01) in micropatterned vs non-patterned hiPSC-CMS detected with ReactomeGSA. Data presented as the average Log2(Fold change).
F. All significantly upwnregulated pathways (FDR<0.01) in micropatterned vs non-patterned hiPSC-CMS detected with ReactomeGSA. Data presented as the average Log2(Fold change).

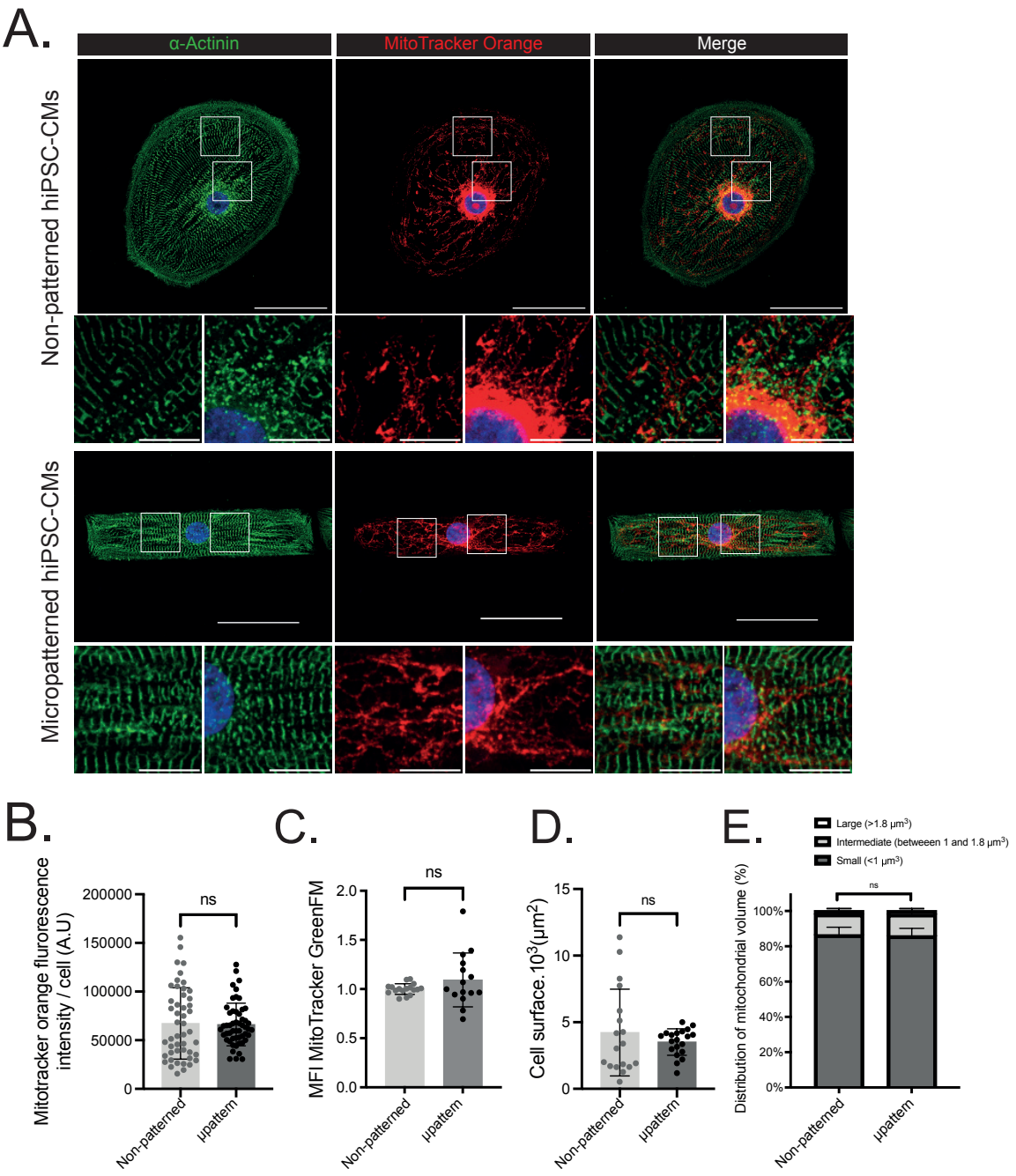


Supplementary Figure 5: Additional results of mitochondrial respiration and glycolytic function in micropatterned hiPSC-CMs compared to non-patterned hiPSC-CMs.

A. Scatter plots show spare respiratory capacity, and proton leak. N = 8-11 differentiations.

B. Quantification of glycolytic reserve in non-patterned and micropatterned group. N = 4-12 differentiations.

Results, mean ± standard deviation. Statistical analyses: Mann-Whitney was used for A and B. * $p<0.05$, ns: not significant, for the indicated comparisons.



Supplementary Figure 6: Mitochondrial network analysis in micropatterned and non-patterned hiPSC-CMs.

A. Non-patterned and micropatterned hiPSC-CMs stained with MitoTracker™ Orange 7 days after seeding. DAPI (blue) was used to stain nuclei. The insert represents a zoomed view of sarcomeres and mitochondrial networks. Global scale bar 50 µm, insert scale bar 10 µm.

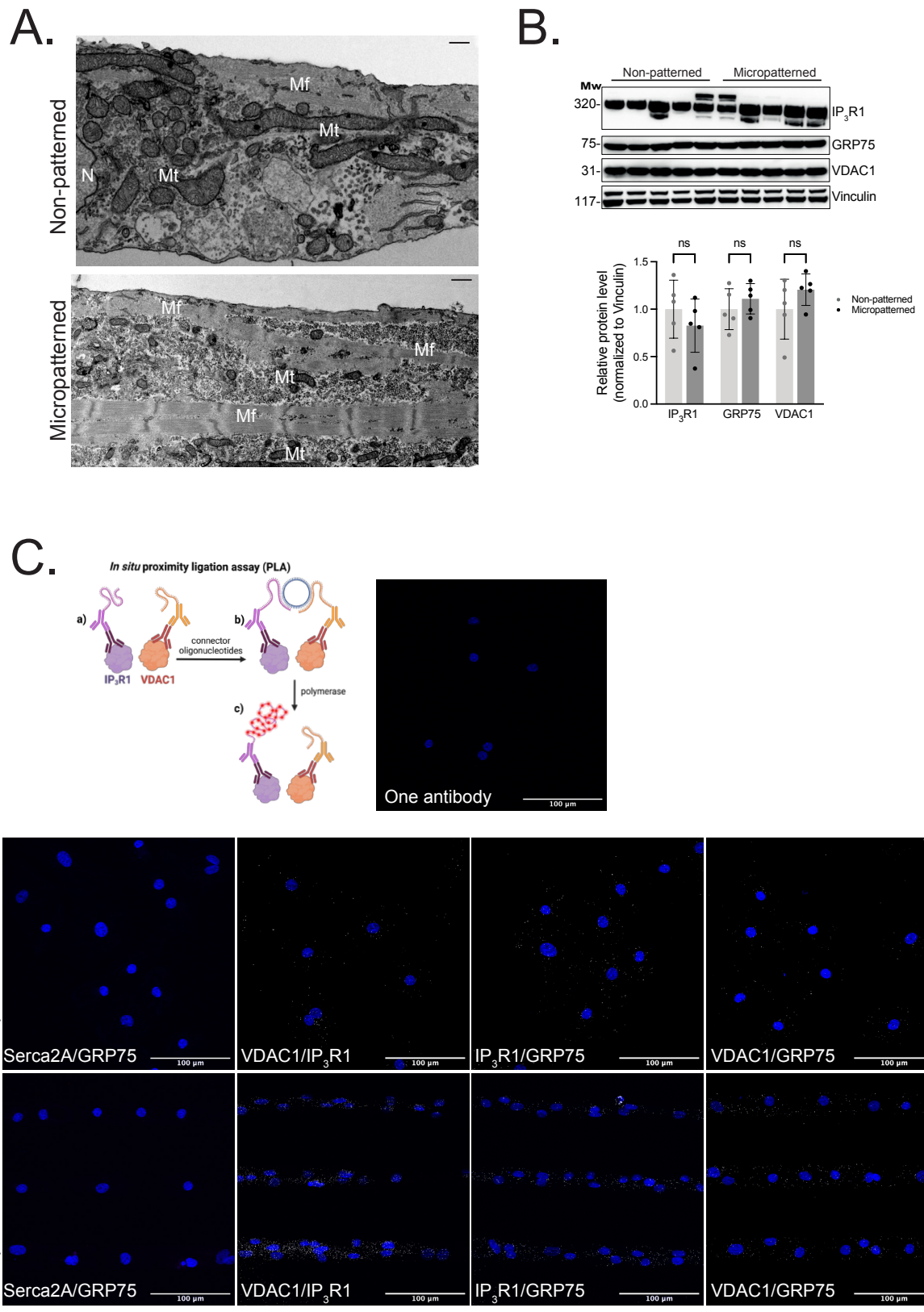
B. Quantitative analysis of MitoTracker™ fluorescence intensity measured with Fiji software. n = 48 non-patterned cells, n = 53 micropatterned cells; N = 3-4 differentiations.

C. Flow cytometry analysis of MitoTracker™ Green in non-patterned and micropatterned hiPSC-CMs. N = 6 differentiations.

D. Scatter plot shows cell surface measured with Fiji software. n = 18 non-patterned cells, n = 20 micropatterned cells; N = 3 differentiations.

E. Distribution of individual mitochondrial volume between small (<1 μm^3), intermediate (between 1 and 1.8 μm^3) or large (>1.8 μm^3) mitochondria evaluated by IMARIS.

Results, mean ± standard deviation. Statistical analyses: Mann-Whitney was used for B through D, Kruskal-Wallis test followed post-hoc Dunn's multiple comparisons test for E. ns: not significant, for the indicated comparisons.



Supplementary Figure 7: Ultra structural characteristics of micropatterned and non-patterned hiPSC-CMs.

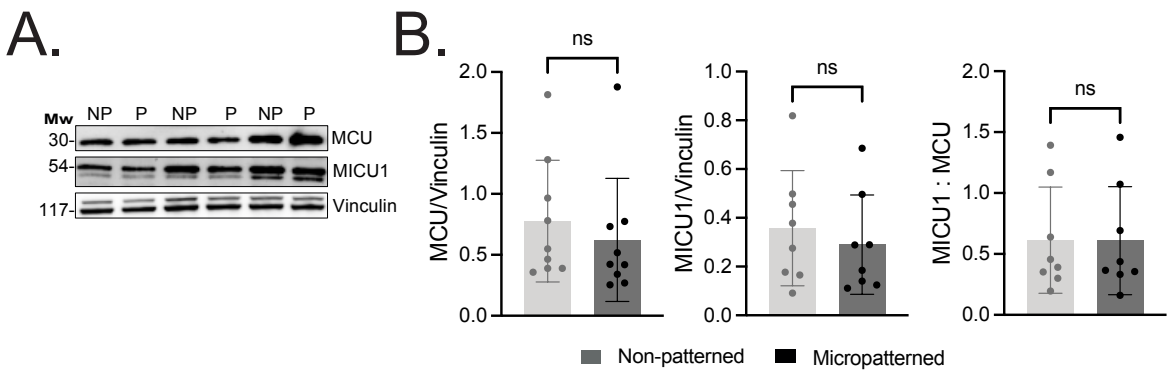
A. Representative TEM images of the cellular structure of non-patterned (top) and micropatterned (bottom) hiPSC-CMs in transverse cross-section; scale = 1 µm. Mf indicates myofibril; Mt mitochondria; and N nucleus.

B. Western blot quantitative analysis of VDAC1, GRP75, and IP_3R1 protein abundance in non-micropatterned and micropatterned hiPSC-CMs. n = 5 differentiations / conditions. Vinculin was used as a loading control.

C. (top) Schematic representation of in situ PLA steps for visualization of VDAC1/IP_3R1 interactions: a) fixed and permeabilized cultured hiPSC-CMs are incubated with two different primary antibodies, one directed against the mitochondrial channel VDAC1 and another one against the IP_3R1 channel in the SR, b) circularization and ligation of connector oligonucleotides of secondary antibodies when proteins are less than 40 nm away, c) rolling circle amplification with polymerase and detection of the product with fluorescent probes. Created with Biorender.com.

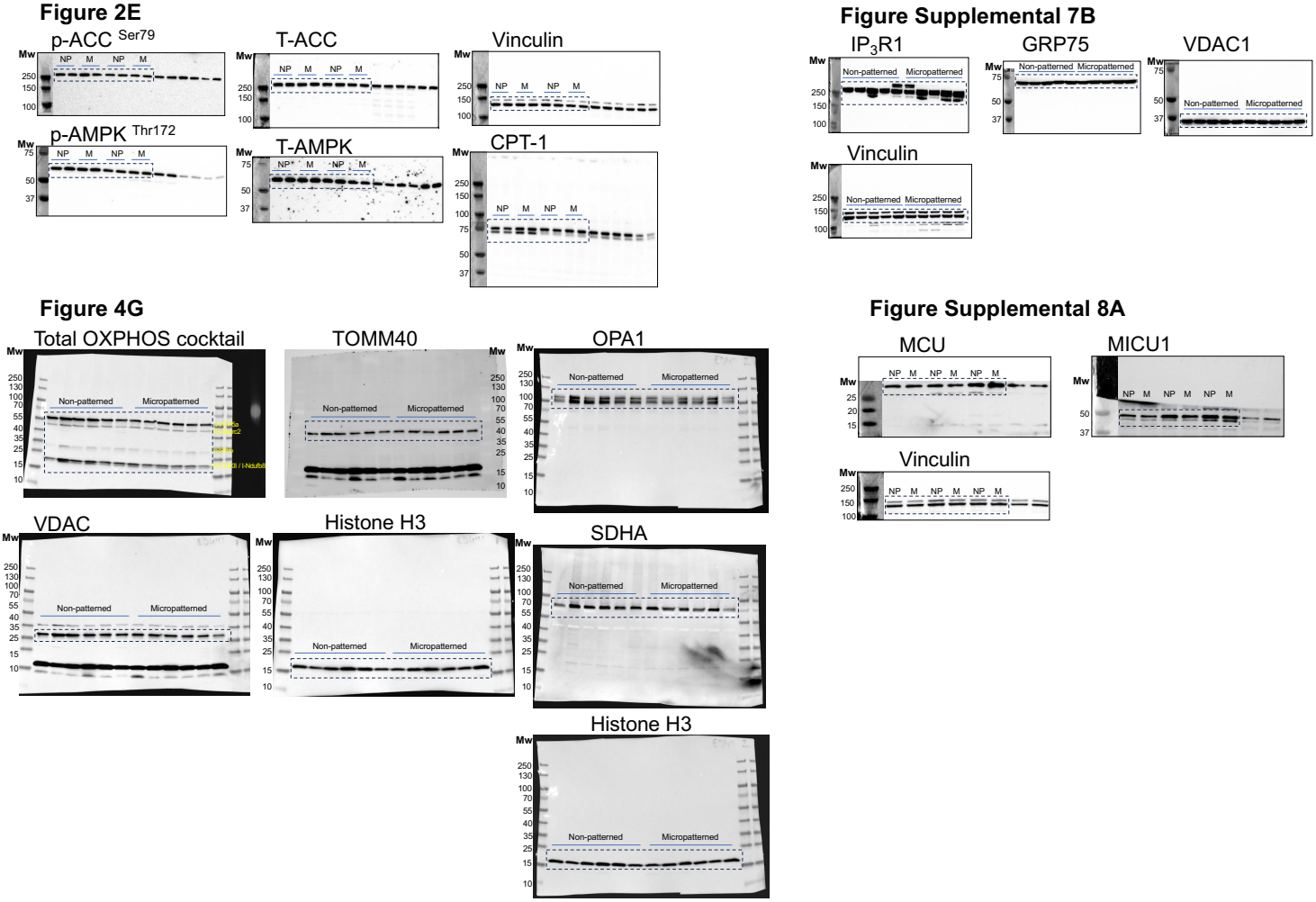
(bottom) Representative images of in situ PLA analysis in hiPSC-CMs cells. Nuclei appear in blue and interactions between two targeted proteins are depicted in whites. IP_3R1 interacts with both VDAC1 and GRP75. As negative controls, we demonstrate that GRP75 do not interacts with Serca2a (another SR membrane protein).

Results, mean ± standard deviation. Statistical analyses: Mann-Whitney test was used for B. ns: not significant for the indicated comparisons.



Supplementary Figure 8: MCU and MICU1 expression.

A. Representative immunoblots for MCU and MICU1.
B. Quantification of relative protein level of MCU and MICU1 in non-patterned and micropatterned hiPSC-CMs. Proteins ratios of MICU1 to MCU was calculated individually for each differentiation (n = 9). Vinculin was used as loading control.
Results, mean ± standard deviation. Statistical analyses: Mann-Whitney test. ns: not significant for the indicated comparisons.



Supplementary Figure 9: Full scans of Western blots reported. Dashed frames indicate the data presented in the manuscript Figures.